Cell Reports, Volume *29*

Supplemental Information

Identification and Analyses of Extra-Cranial and Cranial Rhabdoid Tumor Molecular Subgroups Reveal Tumors with Cytotoxic T Cell Infiltration

Hye-Jung E. Chun, Pascal D. Johann, Katy Milne, Marc Zapatka, Annette Buellesbach, Naveed Ishaque, Murat Iskar, Serap Erkek, Lisa Wei, Basile Tessier-Cloutier, Jake Lever, Emma Titmuss, James T. Topham, Reanne Bowlby, Eric Chuah, Karen L. Mungall, Yussanne Ma, Andrew J. Mungall, Richard A. Moore, Michael D. Taylor, Daniela S. Gerhard, Steven J.M. Jones, Andrey Korshunov, Manfred Gessler, Kornelius Kerl, Martin Hasselblatt, Michael C. Frühwald, Elizabeth J. Perlman, Brad H. Nelson, Stefan M. Pfister, Marco A. Marra, and Marcel Kool

Figure S1

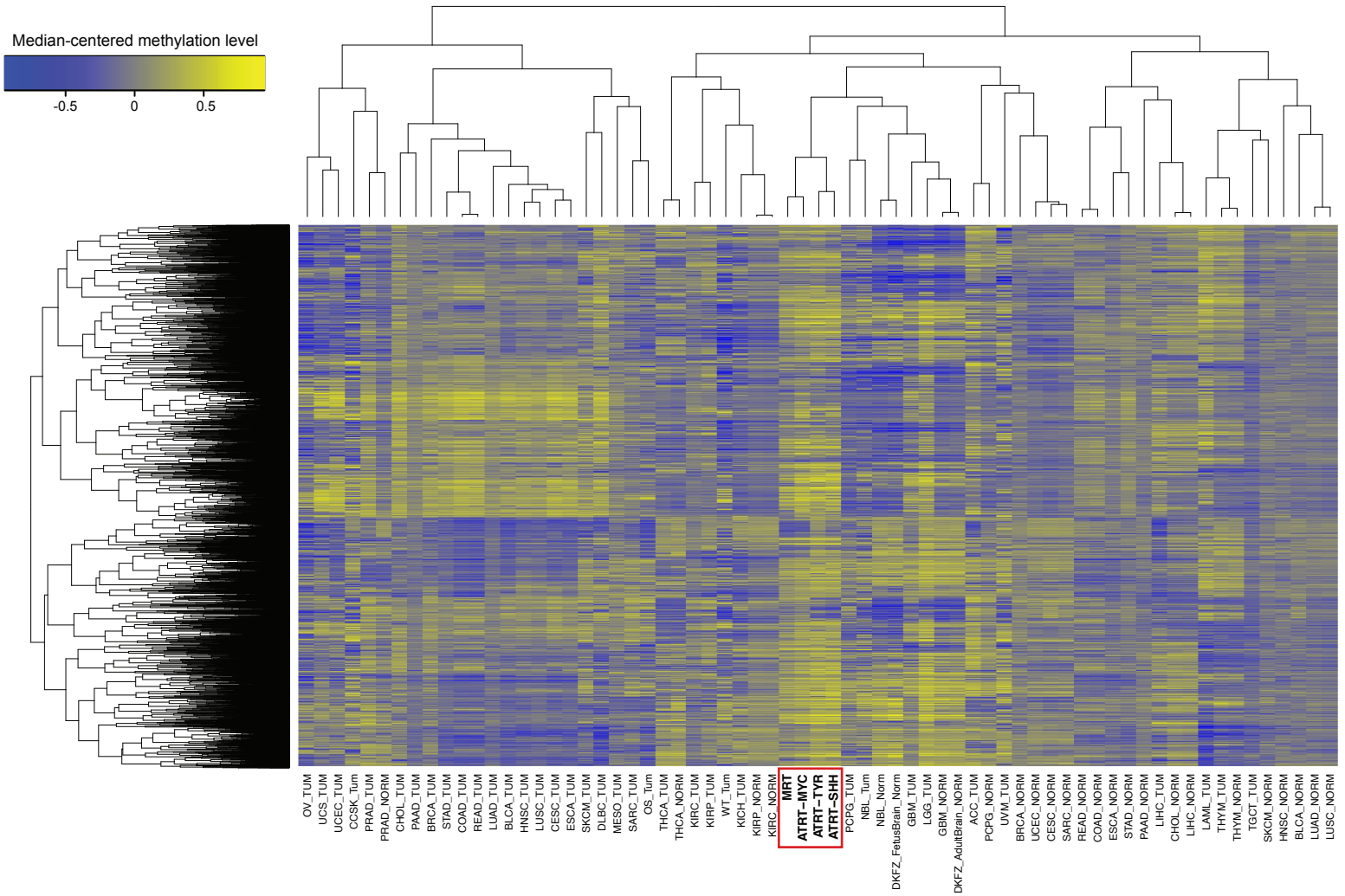

Figure S1. Comparison of DNA methylation profiles from MRTs and ATRTs to TCGA cases revealed that RTs are distinct from adult tumor and differentiated tissue types, and show relative similarities to cancers originating from neural crest-derived cell types, brain cancers and normal brain tissues. Related to Figure 1.

Unsupervised hierarchical clustering of 301 MRT and ATRT cases, 9,757 TCGA cases and 475 TARGET cases representing 33 different tumor types and 23 normal tissue types was performed using DNA methylation array data. Median methylation levels were used to represent each tumor and normal tissue type. The top 8,000 most variable median values were used for the clustering analysis. A suffix, "_TUM", indicates an adult tumor case, whereas "_Tum" denotes a pediatric tumor case. "_NORM" indicates a matched adult normal case, whereas "_Norm" indicates a pediatric normal case. Disease abbreviations are listed in the STAR Methods.

Figure S2

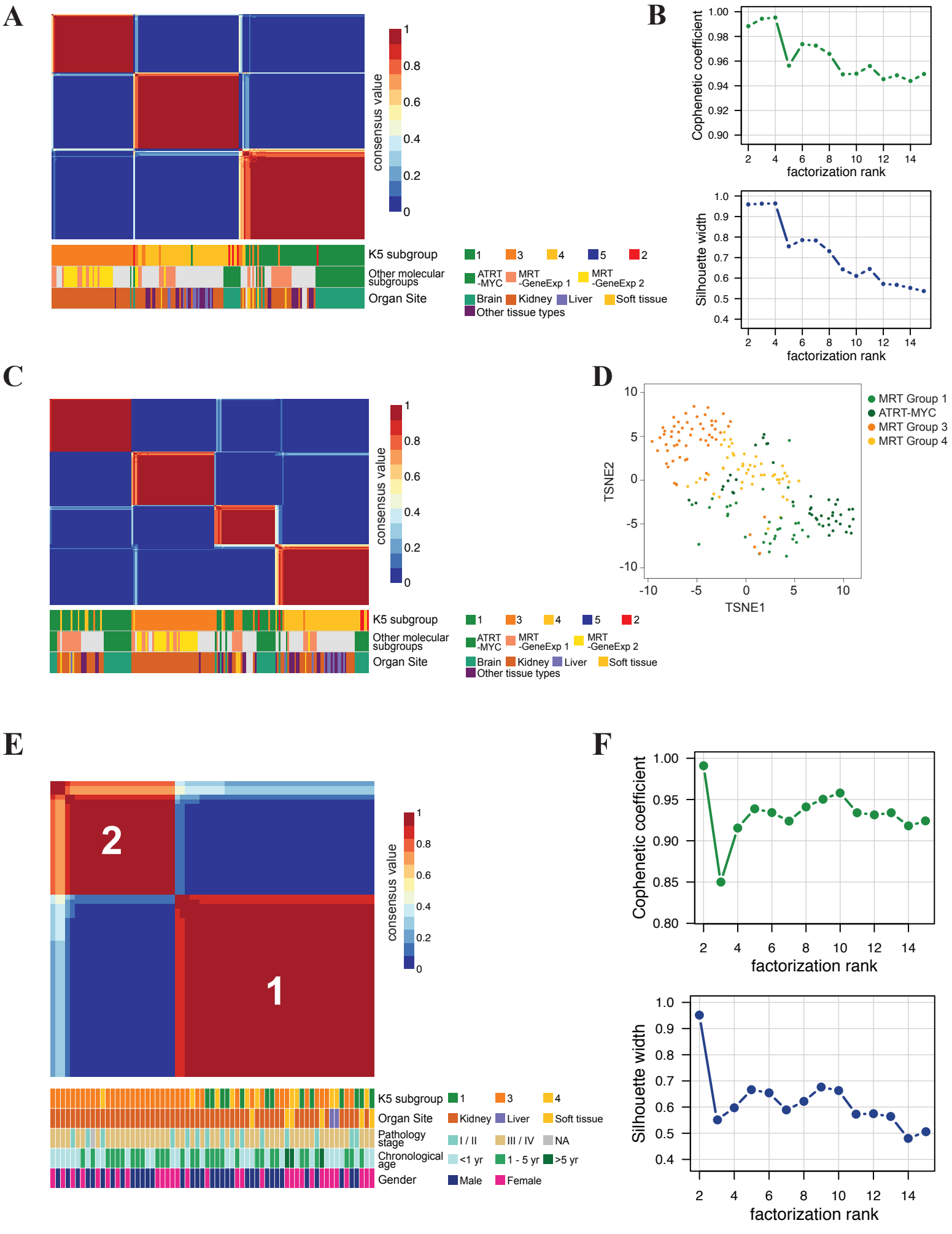
A
consensus value
1
0.8
0.6
0.4
0.2
0
K5 subgroup
1
3
4
5
2
Other molecular subgroups
ATRT -MYC
MRT -GeneExp 1
MRT -GeneExp 2
Organ Site
Brain
Kidney
Liver
Soft tissue
Other tissue types
B
Cophenetic coefficient
factorization rank
Silhouette width
factorization rank
C
consensus value
K5 subgroup
Other molecular subgroups
Organ Site
D
TSNE2
TSNE1
MRT Group 1
ATRT-MYC
MRT Group 3
MRT Group 4
E
2
1
consensus value
K5 subgroup
Organ Site
Pathology stage
I / II
III / IV
NA
Chronological age
<1 yr
1 - 5 yr
>5 yr
Gender
Male
Female
F
Cophenetic coefficient
factorization rank
Silhouette width
factorization rank

Figure S2. Clustering of MRT and ATRT-MYC cases reveals subgroups consistent with the five RT subgroups. Related to Figure 2.

Unsupervised NMF analysis was performed using top 10,000 most variably methylated CpG sites from 140 MRT and 44 ATRT-MYC samples. The analysis revealed the most robust clustering solutions at k=3 **(A)** and k=4 **(C)**. Cophenetic coefficients (top) and silhouette widths (bottom) indicating the robustness of NMF clustering from k=2 to k=15 are shown **(B)**. Clinical information, and previously described ATRT subgroups and MRT gene-expression subgroups (in **Figure S2E**) are shown in colored tracks.

(D) t-SNE analysis was performed using the top 10,000 most variably methylated CpG sites from 140 MRT and 44 ATRT-MYC samples, and supported the existence of Groups 1, 3 and 4 also detected using NMF.

(E) NMF consensus matrix from clustering RNA-Seq data of 65 MRT cases (top). Clinical correlates are shown in the bottom panel. The gene expression subgroup 1 contains all extra-renal MRT cases, while gene expression subgroup 2 exclusively contains RTK cases. Metrics indicating the robustness of clustering solutions from k = 2 to k = 15 are shown in **(F)**.

Figure S3

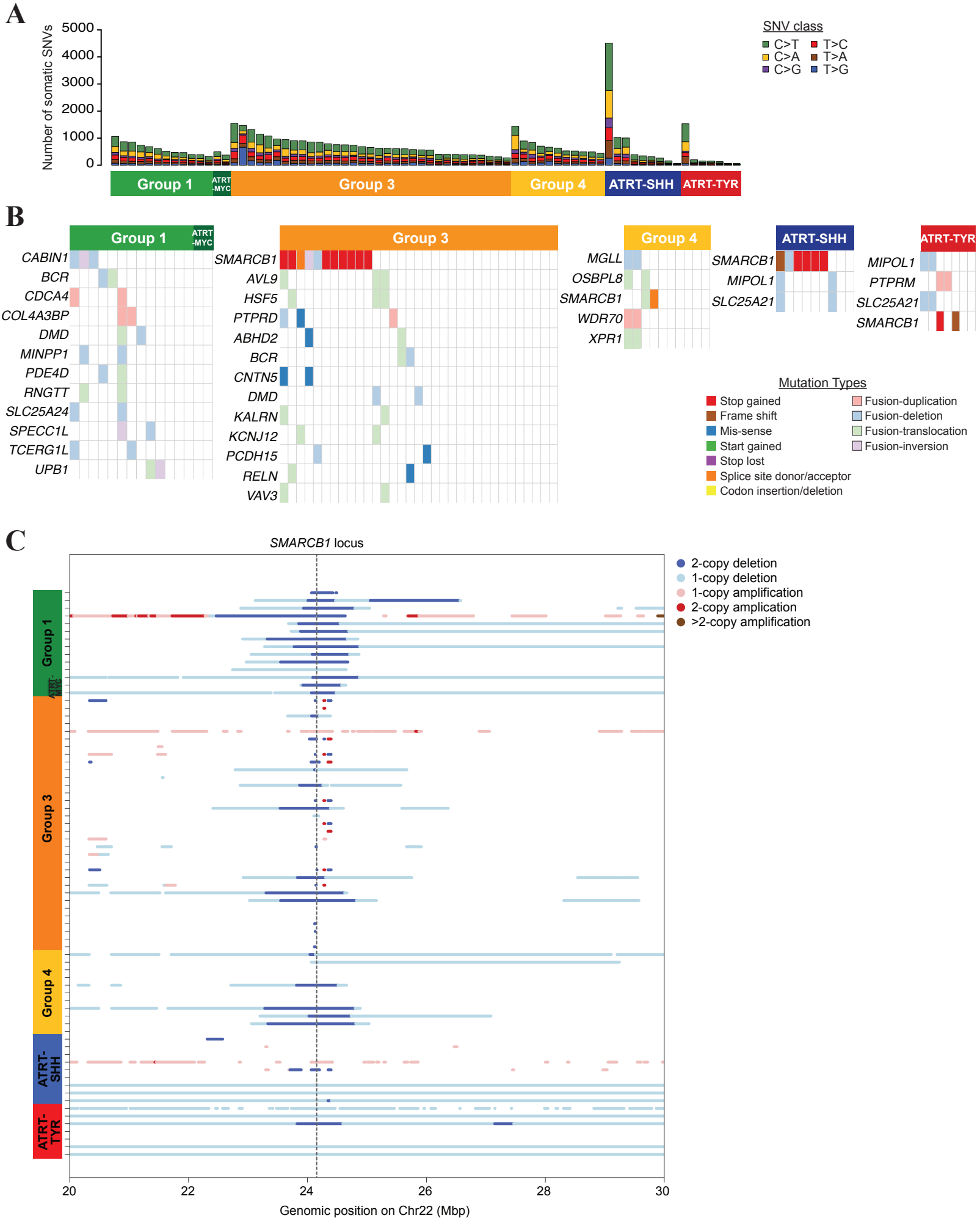
A
Number of somatic SNVs
5000
4000
3000
2000
1000
0
SNV class
C>T
T>C
C>A
T>A
C>G
T>G
Group 1
ATRT-MYC
Group 3
Group 4
ATRT-SHH
ATRT-TYR
B
Group 1
ATRT-MYC
CABIN1
BCR
CDCA4
COL4A3BP
DMD
MINPP1
PDE4D
RNGTT
SLC25A24
SPECC1L
TCERG1L
UPB1
Group 3
SMARCB1
AVL9
HSF5
PTPRD
ABHD2
BCR
CNTN5
DMD
KALRN
KCNJ12
PCDH15
RELN
VAV3
Group 4
MGLL
OSBPL8
SMARCB1
WDR70
XPR1
ATRT-SHH
SMARCB1
MIPOL1
SLC25A21
ATRT-TYR
MIPOL1
PTPRM
SLC25A21
SMARCB1
Mutation Types
Stop gained
Frame shift
Mis-sense
Start gained
Stop lost
Splice site donor/acceptor
Codon insertion/deletion
Fusion-duplication
Fusion-deletion
Fusion-translocation
Fusion-inversion
C
SMARCB1 locus
2-copy deletion
1-copy deletion
1-copy amplification
2-copy amplication
>2-copy amplification
Group 1
ATRT-MYC
Group 3
Group 4
ATRT-SHH
ATRT-TYR
20
22
24
26
28
30
Genomic position on Chr22 (Mbp)

Figure S3. Mutation profiles across RT subgroups. Related to Figure 2.

(A) Barplot shows the number and classes of somatic single nucleotide variants (SNVs) found across RT subgroups.

(B) Oncoprints show recurrently mutated genes across RT subgroups. Different mutation types are indicated by colored boxes for MRT and ATRT cases.

(C) Copy number alteration events at the *SMARCB1* locus (Chr22: 20,000,000 – 30,000,000 bp) across RT subgroups. Somatic copy number alterations were identified using WGS data from 74 tumor-normal pairs.

Figure S4

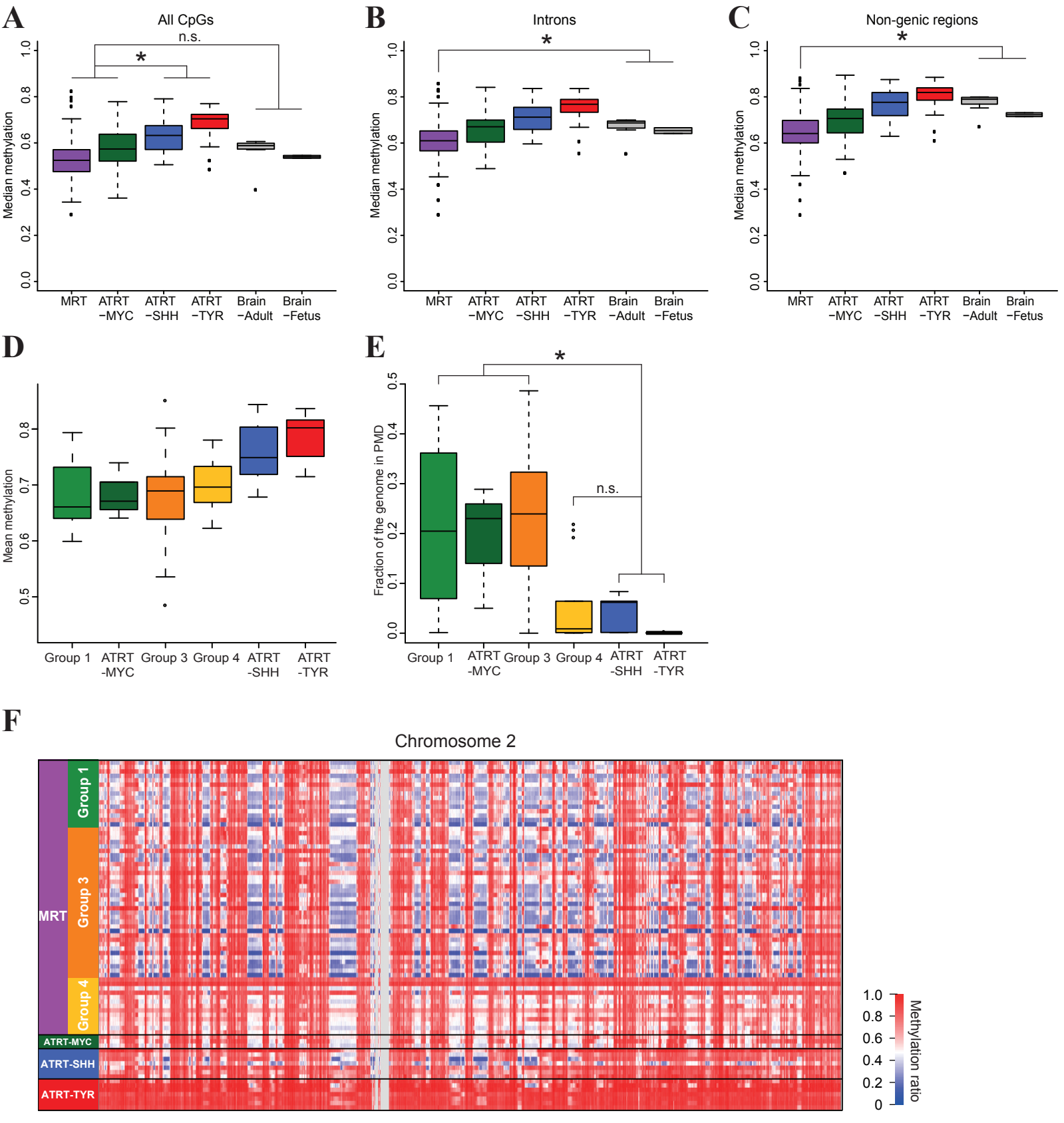
A
All CpGs
n.s.
*
Median methylation
MRT
ATRT −MYC
ATRT −SHH
ATRT −TYR
Brain −Adult
Brain −Fetus
B
Introns
*
C
Non-genic regions
*
D
Mean methylation
Group 1
ATRT -MYC
Group 3
Group 4
ATRT -SHH
ATRT -TYR
E
*
n.s.
Fraction of the genome in PMD
F
Chromosome 2
MRT
Group 1
Group 3
Group 4
ATRT-MYC
ATRT-SHH
ATRT-TYR
Methylation ratio

Figure S4. Analyses of DNA methylation array and WGBS data consistently reveal that MRT and ATRT-MYC cases show relative hypomethylation compared to ATRT-SHH and -TYR cases. Related to Figure 3.

DNA methylation levels were profiled for 301 RT cases and 10 normal brain cases using Illumina 450K and 850K arrays. Boxplots show distributions of median methylation levels of all CpG sites targeted by the arrays **(A)**, median methylation levels in introns of protein-coding genes **(B)**, and in non-genic regions **(C**; * Wilcoxon p-value < 0.05; n.s. = not significant).

(D) Boxplot shows mean global DNA methylation levels based on WGBS data across five RT subgroups.

(E) Boxplot shows the fraction of a genome covered by PMDs across five RT subgroups (* Wilcoxon p-value < 0.05; n.s. = not significant).

(F) Heatmap shows CpG methylation levels across chromosome 2 in RT subgroups using WGBS data (red = 100%; blue = 0% methylation).

Figure S5

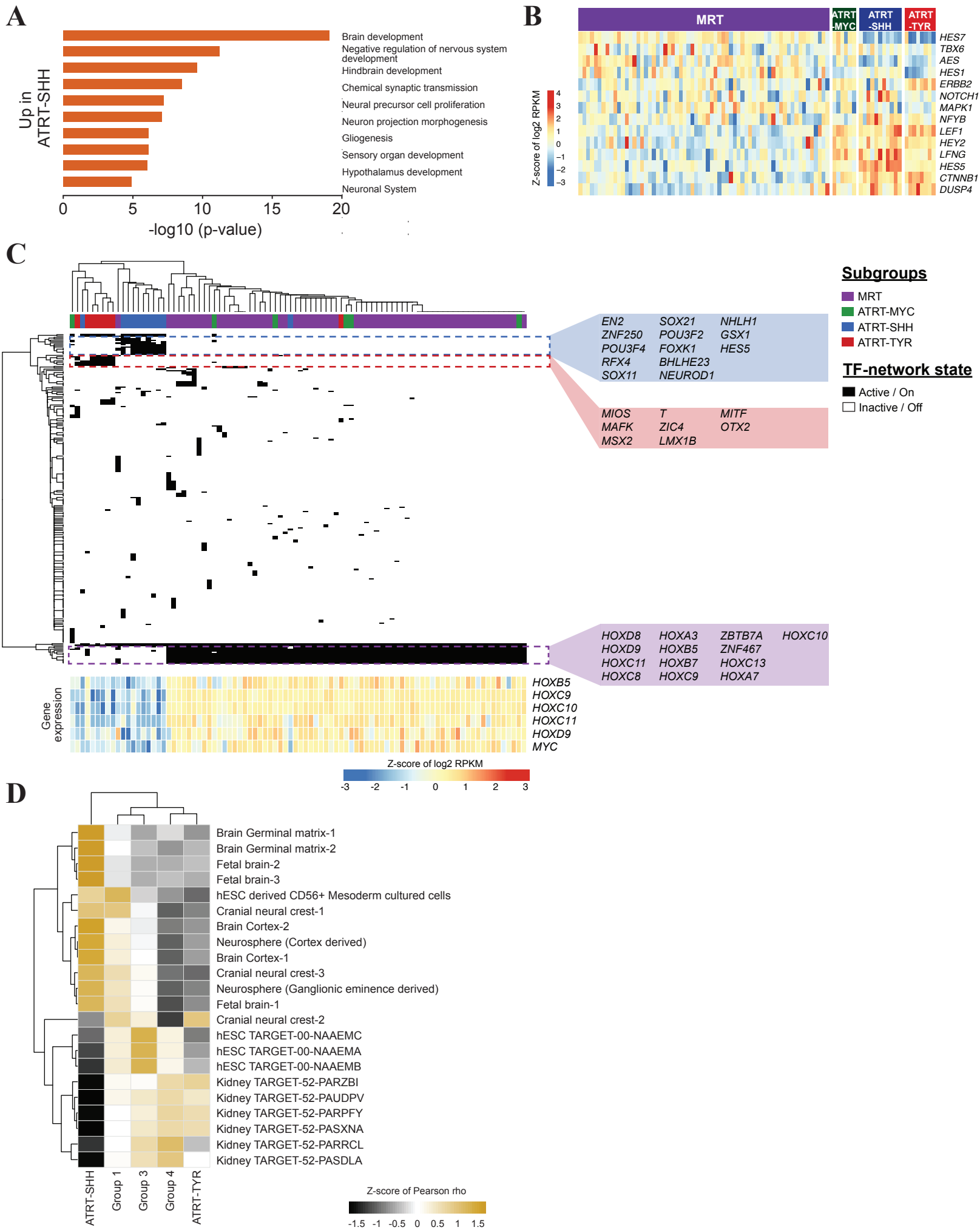
A
Up in ATRT-SHH
Brain development
Negative regulation of nervous system development
Hindbrain development
Chemical synaptic transmission
Neural precursor cell proliferation
Neuron projection morphogenesis
Gliogenesis
Sensory organ development
Hypothalamus development
Neuronal System
0
5
10
15
20
-log10 (p-value)
B
MRT
ATRT -MYC
ATRT -SHH
ATRT -TYR
Z-score of log2 RPKM
4
3
2
1
0
−1
−2
−3
HES7
TBX6
AES
HES1
ERBB2
NOTCH1
MAPK1
NFYB
LEF1
HEY2
LFNG
HES5
CTNNB1
DUSP4
C
Subgroups
MRT
ATRT-MYC
ATRT-SHH
ATRT-TYR
TF-network state
Active / On
Inactive / Off
EN2 SOX21 NHLH1
ZNF250 POU3F2 GSX1
POU3F4 FOXK1 HES5
RFX4 BHLHE23
SOX11 NEUROD1
MIOS T MITF
MAFK ZIC4 OTX2
MSX2 LMX1B
HOXD8 HOXA3 ZBTB7A HOXC10
HOXD9 HOXB5 ZNF467
HOXC11 HOXB7 HOXC13
HOXC8 HOXC9 HOXA7
Gene expression
HOXB5
HOXC9
HOXC10
HOXC11
HOXD9
MYC
Z-score of log2 RPKM
-3 -2 -1 0 1 2 3
D
Brain Germinal matrix-1
Brain Germinal matrix-2
Fetal brain-2
Fetal brain-3
hESC derived CD56+ Mesoderm cultured cells
Cranial neural crest-1
Brain Cortex-2
Neurosphere (Cortex derived)
Brain Cortex-1
Cranial neural crest-3
Neurosphere (Ganglionic eminence derived)
Fetal brain-1
Cranial neural crest-2
hESC TARGET-00-NAAEMC
hESC TARGET-00-NAAEMA
hESC TARGET-00-NAAEMB
Kidney TARGET-52-PARZBI
Kidney TARGET-52-PAUDPV
Kidney TARGET-52-PARPFY
Kidney TARGET-52-PASXNA
Kidney TARGET-52-PARRCL
Kidney TARGET-52-PASDLA
ATRT-SHH
Group 1
Group 3
Group 4
ATRT-TYR
Z-score of Pearson rho
-1.5 -1 -0.5 0 0.5 1 1.5

Figure S5. Analyses of TF-regulatory networks and transcriptome comparisons to different progenitor cell types. Related to Figure 5.

(A) Bar plot shows the significance of a pathway enrichment test (-log10 of p-values) for genes that were over-expressed in ATRT-SHH compared to ATRT-TYR.

(B) Heatmap shows expression levels of genes that interact with *HES7* in MRT and ATRT. Relative over-expression of *HES7* and under-expression of its negative downstream target genes including *LEF1, DUSP4, and CTNNB1* are shown in MRT and ATRT-MYC compared to ATRT-SHH and -TYR.

(C) Unsupervised clustering of enrichment of TF-regulatory networks i.e. groups of TF and genes with TF motifs that show co-expression patterns across MRTs and ATRTs (top panel). ATRT subgroups and MRT cases are indicated by different colors. Networks unique to the ATRT-MYC and MRT group, ATRT-SHH, and ATRT-TYR are indicated in dashed boxes. TFs for these networks are listed in larger fonts. Expression levels of TFs whose regulatory networks contained *MYC* as a putative direct target gene are shown in a heatmap (bottom panel).

(D) Unsupervised hierarchical clustering that compared transcriptome profiles of RTs against various progenitor cell types including human embryonic stem cell (hESC) lines from the TARGET consortium, mesodermal progenitors (i.e. hESC-derived CD56+ mesoderm cultured cells), cranial neural crest cell cultures, neural progenitors (i.e. neurospheres derived from ganglionic eminence and cortex, germinal matrix), fetal brains, adult brains (brain cortex), and pediatric kidneys from the TARGET consortium. Pearson correlation coefficients were transformed to Z scores to show the deviation from the mean for each cell types.

Figure S6

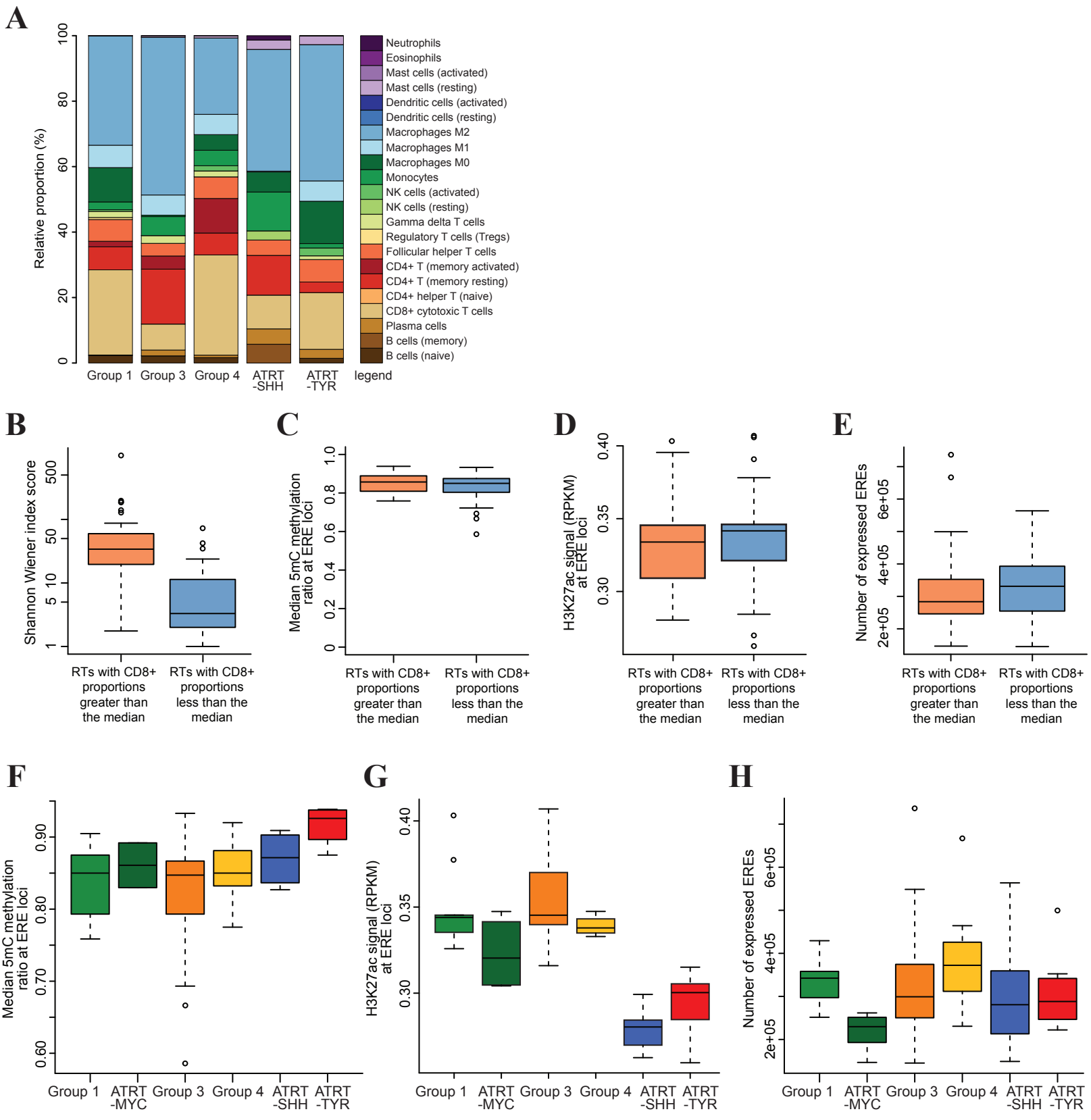
A
Relative proportion (%)
0
20
40
60
80
100
Group 1
Group 3
Group 4
ATRT -SHH
ATRT -TYR
legend
Neutrophils
Eosinophils
Mast cells (activated)
Mast cells (resting)
Dendritic cells (activated)
Dendritic cells (resting)
Macrophages M2
Macrophages M1
Macrophages M0
Monocytes
NK cells (activated)
NK cells (resting)
Gamma delta T cells
Regulatory T cells (Tregs)
Follicular helper T cells
CD4+ T (memory activated)
CD4+ T (memory resting)
CD4+ helper T (naive)
CD8+ cytotoxic T cells
Plasma cells
B cells (memory)
B cells (naive)
B
Shannon Wiener index score
1
5
10
50
500
RTs with CD8+ proportions greater than the median
RTs with CD8+ proportions less than the median
C
Median 5mC methylation ratio at ERE loci
0
0.2
0.4
0.6
0.8
1.0
RTs with CD8+ proportions greater than the median
RTs with CD8+ proportions less than the median
D
H3K27ac signal (RPKM) at ERE loci
0.30
0.35
0.40
RTs with CD8+ proportions greater than the median
RTs with CD8+ proportions less than the median
E
Number of expressed EREs
2e+05
4e+05
6e+05
RTs with CD8+ proportions greater than the median
RTs with CD8+ proportions less than the median
F
Median 5mC methylation ratio at ERE loci
0.60
0.70
0.80
0.90
Group 1
ATRT -MYC
Group 3
Group 4
ATRT -SHH
ATRT -TYR
G
H3K27ac signal (RPKM) at ERE loci
0.30
0.35
0.40
Group 1
ATRT -MYC
Group 3
Group 4
ATRT -SHH
ATRT -TYR
H
Number of expressed EREs
2e+05
4e+05
6e+05
Group 1
ATRT -MYC
Group 3
Group 4
ATRT -SHH
ATRT -TYR

Figure S6. Analyses of tumor purity levels, filtered pathway enrichment, CIBERSORT-based immune cell type deconvolution, and epigenetic profiles at ERE loci. Related to Figure 6.

(A) Stacked bar plot shows relative proportions of 22 immune cell types predicted using CIBERSORT. Boxplots show distributions of Shannon Wiener index scores representing TCR diversity **(B**; higher Shannon Wiener index scores indicate greater TCR diversity); median DNA methylation levels at known ERE loci **(C)**; H3K27ac signal density **(D)**; and numbers of EREs that had normalized read coverage greater then the median (representing the level of transcript abundance in RPM; **E)** in RTs with CD8+ cytotoxic T cell proportions greater or less than the median of the cohort.

Boxplots show distributions of median DNA methylation levels at known ERE loci **(F)**; H3K27ac signal density **(G)**; and numbers of EREs that were expressed at the level greater than the median **(H)** across RT subgroups.

Figure S7

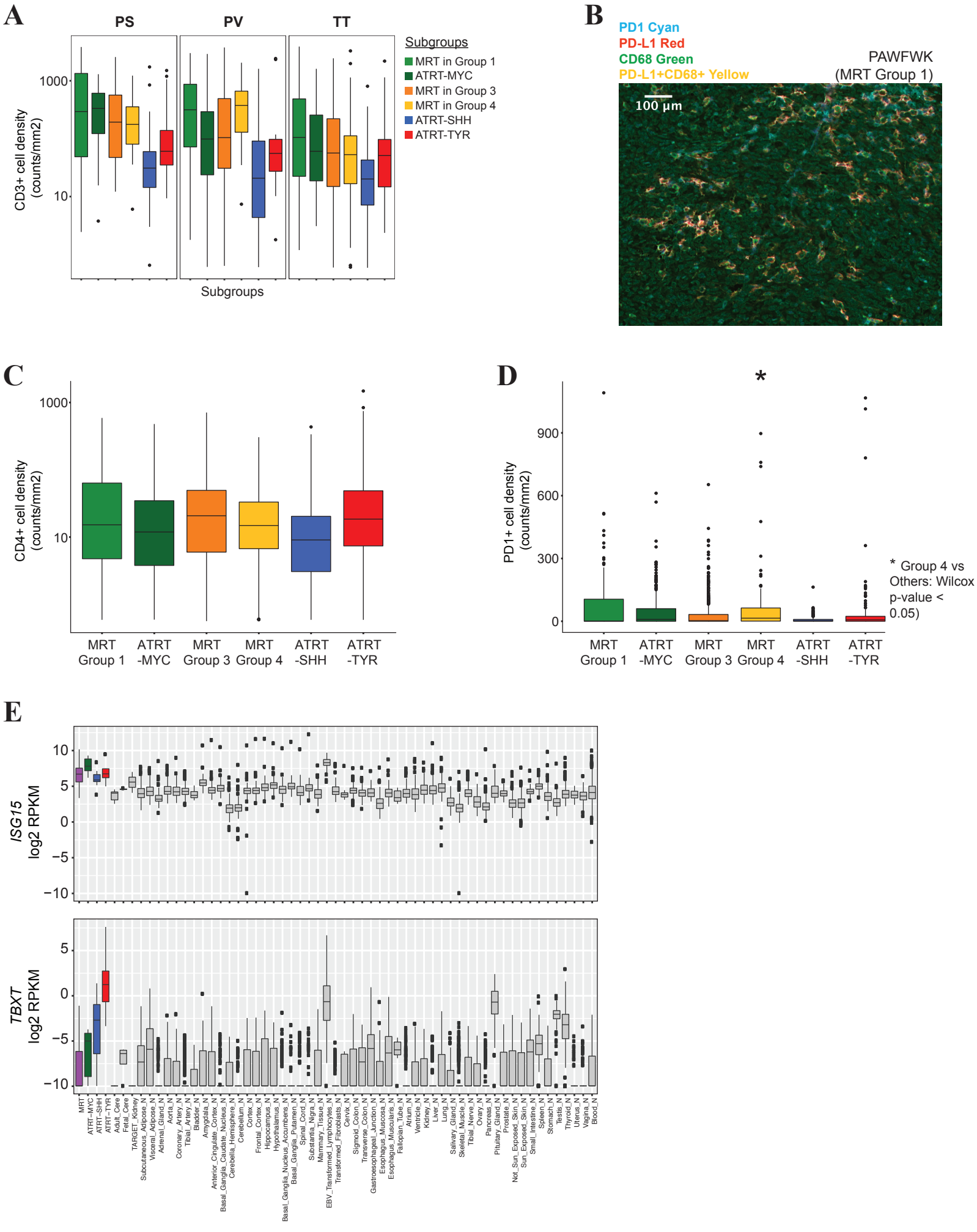
A
PS
PV
TT
Subgroups
MRT in Group 1
ATRT-MYC
MRT in Group 3
MRT in Group 4
ATRT-SHH
ATRT-TYR
CD3+ cell density (counts/mm2)
1000
10
Subgroups
B
PD1 Cyan
PD-L1 Red
CD68 Green
PD-L1+CD68+ Yellow
PAWFWK
(MRT Group 1)
100 µm
C
CD4+ cell density (counts/mm2)
1000
10
MRT Group 1
ATRT -MYC
MRT Group 3
MRT Group 4
ATRT -SHH
ATRT -TYR
D
PD1+ cell density (counts/mm2)
900
600
300
0
*
* Group 4 vs Others: Wilcox p-value < 0.05)
E
ISG15 log2 RPKM
TBXT log2 RPKM
10
5
0
−5
−10

Figure S7. IHC validation experiment results. Related to Figure 7.

(A) Boxplots show distributions of CD3+ leukocyte density (y axis, log10 scale) in tumor-enriched (TT), peri-stromal (PS), and peri-vascular (PV) tissues. MRT cases in Groups 1, 3, 4 and ATRT-MYC cases showed significantly higher CD3+ cell densities compared to ATRT-SHH and -TYR in all regions (Wilcoxon p-values = 1.041e-11, 2.932e-11, and 1.026e-09, respectively). CD3+ T cell density is the sum of CD3+CD8+ and CD3+CD8- cell counts per mm^2.

(B) Example of a case with high PD-L1+ CD68+ immune cell infiltration, revealed by multiplex IHC staining of PD-L1 (red) and CD68 (green). Overlapping colors from PD-L1+CD68+ cells are shown in yellow. A scale bar: 100μm.

(C) Boxplot shows distributions of CD4+ helper T cell densities across MRTs in Groups 1, 3, 4 and ATRT-MYC, -SHH, and -TYR (y axis, log10 scale).

(D) Boxplot shows distributions of PD1-expressing leukocyte densities, with Group 4 exhibiting the highest median level among the RT subgroups (* Wilcoxon p-value < 0.05).

(E) Boxplot distributions of expression levels of *ISG15* (top), and *TBXT* (bottom) across MRT, ATRT-MYC, -SHH, -TYR, adult (n = 5; labeled "Adult_Cere") and fetal cerebellum samples (n = 4; labeled "Fetal_Cere"), normal kidney samples (n = 6; labeled "TARGET_Kidney"), and samples from 52 normal tissue types from GTEx (n = 2,500; with a suffix, "_N").